

UCLA

UCLA Previously Published Works

Title

Dual flip-angle IR-FLASH with spin history mapping for B1+ corrected T1 mapping: Application to T1 cardiovascular magnetic resonance multitasking

Permalink

<https://escholarship.org/uc/item/7k94j11n>

Journal

Magnetic Resonance in Medicine, 86(6)

ISSN

0740-3194

Authors

Serry, Fardad Michael
Ma, Sen
Mao, Xianglun
[et al.](#)

Publication Date

2021-12-01

DOI

10.1002/mrm.28935

Peer reviewed



Published in final edited form as:

Magn Reson Med. 2021 December ; 86(6): 3182–3191. doi:10.1002/mrm.28935.

Dual flip angle (2FA) IR-FLASH with spin history mapping for B₁⁺-corrected T₁ mapping: Application to T₁ cardiovascular magnetic resonance Multitasking

Fardad Michael Serry¹, Sen Ma¹, Xianglun Mao¹, Fei Han², Yibin Xie¹, Hui Han¹, Debiao Li¹, Anthony G. Christodoulou^{1,*}

¹Biomedical Imaging Research Institute, Cedars-Sinai Medical Center, Los Angeles, CA, USA

²Siemens Medical Solutions USA, Inc., Los Angeles, CA, USA

Abstract

Purpose: To develop a single-scan method for B₁⁺-corrected T₁ mapping and apply it for free breathing (FB) cardiac MR Multitasking without electrocardiogram (ECG) triggering.

Methods: One dual-flip-angle (2FA) inversion recovery (IR)-FLASH scan provides two observations of T₁^{*} (apparent T₁) corresponding to two distinct combinations of the nominal flip angle α and B₁⁺. Spatiotemporally co-registered T₁ and B₁⁺ spin history maps are obtained by fitting the 2FA signal model.

T₁ estimate accuracy and repeatability for single-flip-angle (1FA) and 2FA IR-FLASH sequence MR Multitasking were evaluated at 3 Tesla. A T₁ phantom was first imaged on the scanner table, then on two human subjects' thoraxes in both breath-hold (BH) and free-breathing (FB) conditions. IR turbo spin echo (IR-TSE) static phantom T₁ measurements served as reference. In 10 healthy subjects, myocardial T₁ was evaluated with ECG-free, FB Multitasking sequences alongside ECG-triggered BH MOLLI.

Results: For phantom-on-table T₁ estimates, 2FA agreed better with IR-TSE (ICC=0.996, mean error \pm SD = -1.6% \pm 1.9%) than did 1FA (ICC=0.922; mean error \pm SD = -4.3% \pm 12%). For phantom-on-thorax, 2FA was more repeatable and robust to respiration than 1FA (coefficient of variation [CoV]=1.2% 2FA, =11.3% 1FA). In-vivo, in intrasession T₁ repeatability, 2FA (septal CoV=2.4%, 6-segment CoV=4.4%) outperformed 1FA (septal CoV=3.1%, 6-segment CoV=5.5%). In six-segment T₁ homogeneity, 2FA (CoV=7.9%) also outperformed 1FA (CoV=11.1%).

Conclusion: 2FA IR-FLASH improves T₁ estimate accuracy and repeatability over 1FA IR-FLASH, and enables single-scan B₁⁺-corrected T₁ mapping without breath-holds or ECG when used with MR Multitasking.

*Corresponding author: Corresponding Author: Anthony G. Christodoulou, Biomedical Imaging Research Institute, Cedars-Sinai Medical Center, 8700 Beverly Blvd, PACT Ste 400, Los Angeles, CA 90048, Anthony.Christodoulou@cshs.org.

¹-SUPPORTING INFORMATION TEXT for review and publication: Multitasking Acquisition, Reconstruction, T₁/B₁⁺ mapping, and Simulations.

²-SUPPORTING INFORMATION FIGURES WITH CAPTIONS for review and publication: Figures S1, S2, S3, and S4.

Keywords

IR-FLASH; T_1 mapping; B_1^+ map; Look Locker; Cardiac MR; Spin history

1. INTRODUCTION

T_1 maps quantify longitudinal relaxation time T_1 on an absolute scale (typically using inversion recovery¹⁻³ or saturation recovery^{1,4} sequences), enabling objective assessment of tissue status and statistical analysis in longitudinal and multi-center oncological⁵, neurological⁶, abdominal⁷⁻⁸, cardiovascular^{1,9-11} studies, and more. Mapping T_1 in moving organs, e.g., the heart, is challenging, although can be done with prospectively triggered strategies^{2-4,12} or continuous-acquisition techniques which avoid triggering.¹³⁻¹⁸ Continuous acquisition sequences like inversion recovery (IR)-FLASH with a short repetition time (TR) between excitation pulses allow for motion-resolved T_1 mapping in the heart.¹³⁻¹⁸

IR-FLASH T_1 mapping is subject to the Look-Locker effect, which introduces T_1 estimate bias, dependent on the *effective* RF transmit field B_1^+ .¹⁹⁻²⁰ This bias magnifies at B_0 $3T$ ^{10, 19-21} due to the reduced wavelength and greater inhomogeneity of B_1^+ at the tissue. To correct for the bias, a separate pre-scan could in principle be used to map B_1^+ .²²⁻²⁴ However, this map is a snapshot of B_1^+ during a time separate from (and much shorter than) the typical IR period. On the other hand, the Look-Locker-induced bias depends not only on instantaneous B_1^+ , but also the B_1^+ “spin history” (effective B_1^+ experienced by spins as they change location relative to the excitation volume) during the full IR period. A B_1^+ snapshot does not account for this history, which can vary substantially across tissue with motion and/or flow, e.g., with heartbeat, respiration, circulation, and perfusion. Incomplete correction for spin history reduces T_1 mapping reliability. A time-cumulative *effective* (or historical) B_1^+ map, spatiotemporally co-registered with the T_1 map and ideally obtained from the same scan data is therefore preferred.

Expanding upon the authors’ recent conference work,²⁵ this paper describes a method aimed at improving the accuracy and repeatability of T_1 mapping with IR-FLASH, especially under free breathing conditions. The method comprises a dual-flip-angle (2FA) pulse sequence and complementary fitting algorithm for joint T_1 /spin-history mapping. The 2FA IR-FLASH sequence removes the ambiguity in the signal between B_1^+ and T_1 ; the fitting algorithm produces spatiotemporally co-registered spin history and T_1 maps. We evaluate the accuracy and precision of this 2FA IR-FLASH method within the MR Multitasking framework^{13,16}, imaging a static phantom, the phantom on the thoraxes of free-breathing volunteers, and 10 healthy volunteers with cardiac scans.

2. THEORY

Assuming complete gradient spoiling and final approach to steady-state, the IR-FLASH signal equation for the n th readout with excitation repetition time TR and nominal flip angle (FA) α is

$$S[n] = A \sin \alpha \frac{1 - e^{-TR/T_1}}{1 - e^{-TR/T_1} \cos \alpha} \left[1 - (1 - \Pi) \left(e^{-TR/T_1} \cos \alpha \right)^{n-1} \right], \quad (1)$$

where Π accounts for inversion preparation efficiency ($\Pi = -1$ for perfect inversion), and the amplitude A absorbs proton density, T_2^* decay, and receive coil sensitivity. The Look-Locker effect results in a shorter apparent recovery time constant $T_1^* < T_1$.¹⁹ In principle, with perfect prior knowledge of α , for the voxel at position \mathbf{r} , $T_1(\mathbf{r})$ could be calculated by correcting $T_1^*(\mathbf{r})$:

$$\frac{1}{T_1(\mathbf{r})} = \frac{1}{T_1^*(\mathbf{r})} + \frac{\ln \cos \alpha}{TR}. \quad (2)$$

In practice, however, the true α depends on the typically-inhomogeneous B_1^+ amplitude, whose unknown spatial pattern impacts the correction in Equation (2). For small FA $< 30^\circ$,²⁶ the actual (true) FA map $\alpha_{\text{true}}(\mathbf{r})$ is

$$\alpha_{\text{true}}(\mathbf{r}) = \beta(\mathbf{r}) \cdot \alpha, \quad (3)$$

where the dimensionless parameter $\beta(\mathbf{r})$ is the normalized B_1^+ relative to the nominally prescribed FA, such that the true flip angle matches the nominal flip angle wherever $\beta(\mathbf{r}) = 1$. Equation (2) then updates to

$$\frac{1}{T_1(\mathbf{r})} = \frac{1}{T_1^*(\mathbf{r})} + \frac{\ln \cos[\beta(\mathbf{r}) \cdot \alpha]}{TR}, \quad (4)$$

which now has two unknowns: $T_1(\mathbf{r})$ and $\beta(\mathbf{r})$. This ambiguity can be resolved by either: 1) assuming $\beta(\mathbf{r}) = 1$, which introduces bias and error into T_1 mapping; 2) mapping $\beta(\mathbf{r})$ from a separate pre-scan, which is inefficient; or 3) assuming that FLASH excitation pulse B_1^+ efficiency equals inversion pulse B_1^+ efficiency¹⁴, i.e., ($\beta = \text{acos}(\Pi)/\pi$), although the inversion pulse violates the small FA approximation, and may have different properties (e.g., non-selective inversion vs. slice-selective excitation).

Furthermore, none of these strategies addresses the effects of inflow and through-plane respiratory motion on the *effective* B_1^+ experienced by spins in the excited slice. Spins within the excited slice (e.g., myocardial tissue) experience the full set of slice-selective excitation pulses during the recovery period, whereas spins that flow through the slice (e.g., blood) see fewer excitation pulses, experiencing a reduced Look-Locker effect (lower effective B_1^+).

Additionally, through-plane respiratory motion dynamically shifts the slice excitation profile as seen in the reference frame of the spins, further reducing the effective B_1^+ during T_1 recovery. A B_1^+ map reflecting physiological dynamics and the time-cumulative nature of the Look-Locker effect during T_1 relaxation is, then, better suited for correcting the error in T_1^* , improving the fidelity of the resulting T_1 estimate.

A straightforward way to resolve the ambiguity of having two unknowns in Equation (4) would be to repeat the acquisition with a second TR or a second nominal FA, obtaining two different measurements of T_1^* from which to extract the two unknowns: $T_1(\mathbf{r})$, $\beta(\mathbf{r})$. For fast sequences such as used in cardiac MR, TR is typically very short, near the limits of gradient switching and physiological stimulation, so a second TR must necessarily be longer, incurring a time penalty and loss of temporal resolution. Introducing a second nominal excitation FA α_2 is therefore more attractive.

To this end, our proposed 2FA IR-FLASH sequence (Figure 1B) alternates between different nominal FAs α_1 and α_2 during successive IR periods. This interleaved FA pattern is preferred to a non-interleaved pattern (a half-length scan at α_1 followed by a half-length scan at α_2), which would share the same temporal co-registration shortcomings as performing a separate B_1^+ pre-scan. Furthermore, the interleaved FA strategy benefits high-dimensional motion-resolved frameworks, e.g., Multitasking, ensuring for example that each respiratory bin has data from both FAs even with respiratory drift present.

The 2FA IR-FLASH signal equation at the k th IR period can be obtained by updating Equation (1) as

$$S_k[n] = A \sin(\check{\beta}\alpha_k) \frac{1 - e^{-TR/T_1}}{1 - e^{-TR/T_1} \cos(\beta\alpha_k)} \left[1 - (1 - PQ_k) \left(e^{-TR/T_1} \cos(\beta\alpha_k) \right)^{n-1} \right] \quad (5)$$

where Q absorbs the effects of having inverted the magnetization from the previous FA's steady-state. Assuming steady-state established at the final FLASH readout at each FA, Q would be expressed as

$$Q_k = \frac{1 - e^{-TR/T_1} \cos(\beta\alpha_k)}{1 - e^{-TR/T_1} \cos(\beta\alpha_{k-1})}. \quad (6)$$

Both cosine terms in Equation (5) depend on spin history, and thus include the time-cumulative effective B_1^+ parameter, β . However, the sine term depends instead on the *instantaneous* B_1^+ , denoted by the dimensionless parameter $\check{\beta}$ (also normalized relative to the nominal FA). This difference is inconsequential for estimating T_1 , because for small FA, the $\check{\beta}$ in $\sin(\check{\beta}\alpha_k)$ can be absorbed into an apparent amplitude A^* ; i.e., $A \sin(\check{\beta}\alpha_k) \approx A\check{\beta} \sin \alpha_k \equiv A^* \sin \alpha_k$. The revised signal equation is then

$$S_k[n] = A^* \sin \alpha_k \frac{1 - e^{-TR/T_1}}{1 - e^{-TR/T_1} \cos(\beta \alpha_k)} \left[1 - (1 - \Pi \cdot Q_k) \left(e^{-TR/T_1} \cos(\beta \alpha_k) \right)^{n-1} \right]. \quad (7)$$

To illustrate the advantage of 2FA over 1FA IR-FLASH for T_1 mapping, IR curves simulated from Equations (1) and (5) for two different combinations of T_1 and β are shown in Figures 1C–D. The two curves are superimposed for 1FA but separated for 2FA. Furthermore, we hypothesize that because Equation (7) encodes a cumulative history of spins in the excited slice, 2FA is not only more robust than 1FA to B_1^+ inhomogeneity, but also to through-plane motion, e.g., with respiration and flow.

3. METHODS

All scans were performed on a 3.0T scanner (MAGNETOM Vida, Siemens Healthcare, Erlangen, Germany). Informed Consent was obtained for all human subjects in accordance with an Institutional Review Board protocol.

3.1 MR Multitasking

We evaluated 2FA IR-FLASH T_1 mapping using MR Multitasking^{13,16}, a non-ECG free-breathing framework for continuous-acquisition parameter mapping. Multitasking sequences using 1FA and 2FA IR-FLASH sequences were implemented. A low-rank tensor^{27–28} model was used for undersampled reconstruction of an image array with multiple temporal dimensions, here chronicling T_1 relaxation, respiration, and cardiac motion. Additional detail is available in the Supporting Information and cited references.^{13,16}

3.2 In-vitro Methods

We assessed T_1 measurement agreement of 1FA (with and without a pre-scan-derived B_1^+ correction) and 2FA IR-FLASH Multitasking sequences with an IR-turbo spin echo (IR-TSE) reference sequence, by imaging on the scanner table a static phantom consisting of 13 vials of gadolinium-doped water surrounded by an undoped water matrix. Within-vial T_1 standard deviations (SDs) measured 1FA and 2FA precision difference. We also assessed the impact of respiration on 1FA and 2FA measurements by placing the same phantom on the thoraxes of two subjects, scanning it under both breath-hold (BH) and free-breathing (FB) conditions. For the first volunteer, both scans were performed twice to further assess repeatability.

Sequence parameters for both IR-FLASH scans were: non-selective inversion pulse; IR recovery period=2.5s; $TR=3.6$ ms; $T_E=1.6$ ms; $FOV=270$ mm \times 270mm; matrix size=160 \times 160; spatial resolution=1.7mm \times 1.7mm; slice thickness=8mm. For 1FA scans, $\alpha=5^\circ$; for 2FA scans, $\alpha_1=3^\circ$, $\alpha_2=10^\circ$, chosen to minimize the Cramér-Rao bound on myocardial T_1 variance. For both 1FA and 2FA, acquisition time=60s for static and FB scans, and 17s for BH scans. IR-TSE sequence parameters were: $TR=8$ s; Echo spacing=9.8ms; TurboFactor=8; $T_E=9.8$ ms; $TI=25, 250, 750, 1000, 1250, 1500, 1750, 2000, 3000, \text{ and } 4000$ ms; $FOV=225$ mm \times 225mm; matrix size=256 \times 256; spatial resolution=0.9mm \times 0.9mm; slice

thickness=8mm; total acquisition time=26 minutes (156s per TI). To compare the overall trend of B_1^+ inhomogeneity, a separate B_1^+ map was also obtained for the static scan with a pre-saturation-based B_1^+ pre-scan provided by the scanner manufacturer.²⁹

IR-FLASH images were reconstructed with the MR Multitasking framework, with only a T_1 recovery time dimension for the static and BH cases, and with an additional respiratory dimension (6 bins) for the FB cases; the number of spatial basis functions (spatial rank) was 7 for in-vitro scans. For 1FA, three-parameter non-linear least-squares (NLLS) fitting of T_1 , A , and Π , to Equation (1) assumed fixed nominal FA. For 2FA, four-parameter NLLS fitting of two concatenated instances of Equation (7) ($k=1, 2$) was performed, fitting T_1 , β , A^* , and Π . Q was re-derived symbolically to additionally account for incomplete steady-state. Both fitting procedures included slice profile correction with 5 sub-slices.³⁰

3.3 In-vivo Methods

To assess in-vivo performance of myocardial T_1 mapping, we imaged $n=10$ healthy adult subjects, scanned with MOLLI, followed by 60s 1FA and 60s 2FA IR-FLASH Multitasking scans. A short-axis mid-ventricular slice was scanned twice with each protocol in 9 subjects and, time constrained, once in a 10th. MOLLI reference maps were acquired at an end-expiration BH at end-diastole. MOLLI scan parameters: FOV=306mm×360mm, matrix size=218×256; spatial resolution=1.4mm×1.4mm; slice thickness=8mm.

Multitasking reconstruction of IR-FLASH images used a T_1 recovery time dimension, a respiratory dimension (6 bins), and a cardiac dimension (20 cardiac phases); the spatial rank was 40. A wavelet denoising parameter was determined by visual inspection on a representative subject, and then used for all subjects (Supporting Information Figure S4). Unlike MOLLI, fitted 1FA and 2FA T_1 maps were cardiac- and respiratory-resolved, so the end-expiration, end-diastolic phases were extracted for comparison. Measurements from six mid-ventricular myocardial segments were taken from conservative ROIs to avoid partial volume effects.

3.4 Statistical Analysis

Intraclass correlation coefficient (ICC) was computed according to Watson.³¹ Coefficient of variation (CoV) for one pair of T_1 values is the SD divided by the mean. For a group of pairs (aggregate CoV), it is the root mean square of pairwise CoVs. In-vitro, we calculated BH-FB CoV (variation of pairwise BH-FB measurements) to measure the impact of free-breathing, and total CoV (variation across all 6 phantom-on-thorax scans) as a measure of reproducibility. In-vivo, we calculated intrasession CoV (variation of measurements from two scans) in each myocardial segment as a measurement of repeatability, and left ventricular (LV) intersegment CoV (variation of segmental means) as a measure of spatial inhomogeneity. Bias and limits of agreement were, respectively, the mean of differences and ± 1.96 times the SD of differences. Statistics reporting follows guidelines in Cole.³²

3.5 Statement on Code Availability

MATLAB (The MathWorks Inc. Natick, MA) reconstruction and fitting P-code is available from the corresponding author upon reasonable request.

4. RESULTS

4.1 In-vitro Results

For the phantom-on-table experiment, 1FA T_1 estimates for the water matrix surrounding the vials decreases from the periphery to the center, Figure 2B. This pattern is mirrored in the reference B_1^+ map, Figure 2D, where B_1^+ increases from the periphery to the center, suggesting B_1^+ inhomogeneity as the source of 1FA T_1 mapping error. Similarly, 1FA substantially underestimates T_1 in the center three vials (IR-TSE T_1 =1486ms, 1563ms, 1780ms), accounting for most of the disagreement between 1FA and IR-TSE estimates seen in Figure 3. In contrast, the 2FA water matrix T_1 is relatively uniform in Figure 2C. It is instead the 2FA spin history β map, Figure 2F, which mimics the B_1^+ pre-scan pattern, as desired. The Bland–Altman and scatter plots in Figure 3 confirm that 2FA agreed better with IR-TSE (ICC=0.996, bias \pm limits of agreement= $-1.6\% \pm 1.9\%$ or -21 ± 10 ms) than did 1FA (ICC=0.922, bias \pm limits of agreement= $-4.3\% \pm 11.6\%$ or -63 ± 57 ms). Although agreement between 1FA and IR-TSE improved with pre-scan-derived B_1^+ correction (Supporting Information, Figure S1), 2FA values agreement remained better. Within-vial SDs showed no significant difference between 1FA and 2FA ($p=0.87$), but difference in SDs was correlated with β such that 2FA was more precise when $\beta < 1.04$ (Supporting Information, Figure S2).

For the phantom-on-thorax experiments, IR-FLASH agreement with IR-TSE is depicted in Figures 4A–B for 6 scans each: 2 BH and 2 FB in the same session (Subject 1), and another 1 BH and 1 FB in a separate session (Subject 2). Comparing FB to BH scans in Figures 4C–D, agreement was better in 2FA (the 3 paired BH and FB ICCs ranged 0.988–0.996) than in 1FA (paired BH and FB ICCs ranged 0.40–0.96). In both overall (6-scan) repeatability and in paired BH-to-FB comparisons, 2FA repeatability outperformed 1FA (total CoV=11.3% 1FA, =1.2% 2FA; BH-FB CoV range =2.7%–13.8% 1FA, =1%–1.5% 2FA), showing 2FA was more robust to respiratory motion, as hypothesized.

4.2 In vivo Results

For subject 3, Figures 5A–D, the 2FA T_1 map identifies right ventricular myocardium better than the 1FA map. For subject 4, Figures 5E–H, the 2FA T_1 map is more homogeneous in LV myocardium than the 1FA map, with inhomogeneity absorbed into the β map instead. This is especially pronounced in the anterolateral LV myocardium (where there is typically an abrupt susceptibility change due to the heart-lung interface). Both subjects' 2FA β maps are darker in the blood pool than in myocardium, reflecting reduced time-cumulative B_1^+ experienced by inflowing blood.

Across 19 scans of 10 volunteers, septal T_1 mean \pm SD was 1240 \pm 37ms for MOLLI, 1633 \pm 167ms for 1FA IR-FLASH, and 1610 \pm 135ms for 2FA IR-FLASH. For the 9 volunteers scanned twice, intrasession CoVs (septal, 6-segment aggregate) were (0.56%, 1.4%) for MOLLI, (3.1%, 5.5%) for 1FA, and (2.4%, 4.4%) for 2FA. Across the 19 scans, intersegment CoVs were 2.8% for MOLLI, 11.1% for 1FA IR-FLASH and 7.9% for 2FA IR-FLASH. Supporting Information Figure S3 shows statistics for each segment.

5. DISCUSSION

Regardless of phantom experiment type (static, BH, FB) 2FA IR-FLASH T_1 estimates agreed with reference IR-TSE better than 1FA estimates did. In phantom-on-thorax (BH, FB) and in vivo scans, 2FA estimated T_1 more repeatably and homogeneously than 1FA.

Recent parallel conference work³³ implemented two separate three-parameter fits to obtain two estimates $T_{1,1}^*$ and $T_{1,2}^*$ from signals at FAs α_1 and α_2 , and computed T_1 and B_1^+ from two instances of Equation (4). In that work, the two different FA scans were performed sequentially in contrast to the interleaved FA scheme performed here and motivated in the Theory section. Direct comparison of these approaches may be warranted in future studies.

5.1 Static Phantom

By fitting concurrently for T_1 and β from the same scan data, 2FA IR-FLASH removes the artefactual variation seen in the 1FA T_1 map and absorbs it into the β map, thus compensating the Look–Locker error due to nonuniform B_1^+ and producing T_1 estimates closer to the IR-TSE estimates.

5.2 Phantom on Thorax

T_1 estimates from 2FA exhibited less variability with respect to respiratory patterns and conditions than estimates from 1FA, as evidenced by the lower CoVs. Furthermore, when directly comparing paired BH-vs.-FB T_1 estimates, 2FA produced higher ICC values, lower biases, and tighter limits of agreement. Overall, these results indicate that 2FA improves robustness to FB conditions, reducing the measurement variability that comes in-part with different subject's respiration patterns and breath holding instruction compliance.

5.3 In vivo Cardiac

Septal T_1 estimates obtained with 2FA IR-FLASH (1610 ± 135 ms) were higher than with MOLLI (1240 ± 37 ms), which is known to underestimate T_1 ,¹⁰ but were closer to values reported at 3T for SAPHIRE (1578 ± 42 ms) and SASHA (1523 ± 46 ms),³⁴ which are considered more accurate than MOLLI. Septal T_1 estimates obtained with 1FA (1633 ± 167 ms) were higher than in previous 1FA IR-FLASH literature¹⁶ that did not include slice profile correction, but were also close to the SAPHIRE and SASHA ranges. A direct comparison of 2FA IR-FLASH to SAPHIRE and/or SASHA is warranted as a subject of future study.

The Look–Locker effect scales with the number of experienced excitation pulses. Stationary isochromats experience more excitation pulses, thus reaching steady-state faster than moving isochromats that experience fewer excitations. In 2D scans, transient blood flowing through the slice experiences fewer excitation pulses than the myocardium resident in the slice, therefore leading to a lower cumulative B_1^+ . The 2FA cardiac β maps reflect this feature; the blood pool has lower β than the surrounding myocardium. Accordingly, 2FA's T_1 estimate of the blood pool is closer to the published range than 1FA's. Since β is influenced by flow, there is a potential for physiological information to be embedded in this map that we are not

currently using, but which future studies may explore, including time-dependent modeling of β to include the expected flow velocities in systole and diastole.

Separately, in Figure 5, β maps are smoother than their 2FA T_1 complements. This is presumably because β values are time-cumulative (historical) measures of the excitation pulses (>8000 in a 1-minute scan) experienced at the corresponding voxels during multiple repetitions of consecutive T_1 recovery periods, each alone longer than a mapped cardiac phase. Also β , a measure of a magnetic field strength, may be expected to vary smoothly absent abrupt, large susceptibility variations across tissue. Notably, the β map records larger B_1^+ experienced by spins in the anterolateral region of the myocardium (arrow in Figure 5H), possibly from abrupt susceptibility change across the myocardium/lung boundary. 1FA T_1 map underestimates T_1 in this region (arrow in Figure 5F). This artefact is absent in 2FA T_1 and MOLLI T_1 maps. As with the phantom, 2FA has absorbed the error in the 1FA T_1 estimate into the β map, rendering T_1 more uniform across the myocardium. Regional analyses confirmed 2FA outperformed 1FA in T_1 measurement homogeneity in healthy volunteers, especially the variation between anterior and lateral segments versus septal segments (Supporting Information Figure S3B).

We evaluated 2FA IR-FLASH using the Multitasking framework. Other continuous-acquisition T_1 mapping frameworks, e.g., TOPAZ¹⁴ and those by Becker et al.^{15,18} have used short 1FA IR-FLASH breath-hold scans, avoiding respiratory-related B_1^+ /spin-history effects. However, they adjusted for other B_1^+ /spin-history effects by assuming the same B_1^+ correction factor for the IR pulse and FLASH pulses¹⁴ or fitting the FA while assuming perfect inversion¹⁸. The basic 2FA concept is compatible with these frameworks and others, and may therefore benefit their future implementations.

CONCLUSIONS

The 2FA IR-FLASH method eliminates the need for a separate scan to obtain a B_1^+ map, and produces a B_1^+ spin history map spatially and temporally co-registered with the T_1 map from the same scan data. This spin history mapping compensates for T_1 estimation errors from inhomogeneous RF pulses and the Look-Locker effect, and reduces T_1 estimate variability from respiration-induced through-plane motion. As a result, T_1 mapping with 2FA IR-FLASH is more accurate and repeatable than with 1FA IR-FLASH.

Supplementary Material

Refer to Web version on PubMed Central for supplementary material.

ACKNOWLEDGEMENTS

This work was supported by NIH R01 EB028146 and NIH R01 HL156818. The authors acknowledge with gratitude the support of Cedars-Sinai Medical Center Research Imaging Core staff.

REFERENCES

1. Kellman P, Hansen MS. T1-mapping in the heart: accuracy and precision. J Cardiovasc Magn Reson. 2014;16:2. 10.1186/1532-429X-16-2 [PubMed: 24387626]

2. Messroghli DR, Radjenovic A, Kozerke S, Higgins DM, Sivananthan MU, Ridgway JP. Modified Look-Locker inversion recovery (MOLLI) for high-resolution T-1 mapping of the heart. *Magn reson med.* 2004;52(1):141–146. 10.1002/mrm.20110 [PubMed: 15236377]
3. Piechnik SK, Ferreira VM, Dall'Armellina E, Cochlin LE, Greiser A, Neubauer S, et al. Shortened Modified Look-Locker Inversion recovery (ShMOLLI) for clinical myocardial T1-mapping at 1.5 and 3 T within a 9 heartbeat breathhold. *J Cardiovasc Magn Reson.* 2010 11 19;12:69. 10.1186/1532-429X-12-69 [PubMed: 21092095]
4. Chow K, Flewitt JA, Green JD, Pagano JJ, Friedrich MG, Thompson RB. Saturation recovery single-shot acquisition (SASHA) for myocardial T(1) mapping. *Magn reson med.* 2014;71(6):2082–95. 10.1002/mrm.24878 [PubMed: 23881866]
5. Lescher S, Jurcoane A, Veit A, Bahr O, Deichmann R, Hattungen E. Quantitative T1 and T2 mapping in recurrent glioblastomas under bevacizumab: earlier detection of tumor progression compared to conventional MRI. *Neuroradiology.* 2015;57(1):11–20. 10.1007/s00234-014-1445-9 [PubMed: 25287076]
6. Maier IL, Hofer S, Eggert E, Schregel K, Psychogios MN, Frahm J, et al. T1 Mapping Quantifies Spinal Cord Compression in Patients With Various Degrees of Cervical Spinal Canal Stenosis. *Front Neurol.* 2020;11:574604. 10.3389/fneur.2020.574604 [PubMed: 33193022]
7. Ashihara N, Watanabe T, Kako S, Kuraishi Y, Ozawa M, Shigefuji S, et al. Correlation of Pancreatic T1 Values Using Modified Look-Locker Inversion Recovery Sequence (MOLLI) with Pancreatic Exocrine and Endocrine Function. *J Clin Med.* 2020;9(6):1085. 10.3390/jcm9061805
8. Gilligan LA, Dillman JR, Tkach JA, Xanthakos SA, Gill JK, Trout AT. Magnetic resonance imaging T1 relaxation times for the liver, pancreas and spleen in healthy children at 1.5 and 3 tesla. *Pediatr Radiol.* 2019;49(8):1018–1024. 10.1007/s00247-019-04411-7 [PubMed: 31049609]
9. Heidenreich JF, Weng AM, Donhauser J, Greiser A, Chow K, Nordbeck P, et al. T1- and ECV-mapping in clinical routine at 3 T: differences between MOLLI, ShMOLLI and SASHA. *BMC Med Imaging.* 2019;19(1):59. 10.1186/s12880-019-0362-0 [PubMed: 31370821]
10. Kellman P, Hansen MS. T1-mapping in the heart: accuracy and precision. *J Cardiovasc Magn Reson.* 2014;16:2. 10.1186/1532-429X-16-2 [PubMed: 24387626]
11. Puntmann VO, Peker E, Chandrashekar Y, Nagel, E. T1 Mapping in Characterizing Myocardial Disease: A Comprehensive Review. *Circ Res.* 2016;119(2):277–99. 10.1161/CIRCRESAHA.116.307974 [PubMed: 27390332]
12. Messroghli DR, Greiser A, Frohlich M, Dietz R, Schulz-Menger J. Optimization and validation of a fully-integrated pulse sequence for modified look-locker inversion-recovery (MOLLI) T1 mapping of the heart. *J Magn Reson Imaging.* 2007;26(4):1081–6. 10.1002/jmri.21119 [PubMed: 17896383]
13. Christodoulou AG, Shaw JL, Nguyen C, Yang Q, Xie YB, Wang N, Li DB. Magnetic resonance multitasking for motion-resolved quantitative cardiovascular imaging. *Nat Biomed Eng.* 2018;2(4):215–226. 10.1038/s41551-018-0217-y [PubMed: 30237910]
14. Weingärtner S, Shenoy C, Rieger B, Schad LR, Schulz-Menger J, Akçakaya M. Temporally resolved parametric assessment of Z-magnetization recovery (TOPAZ): Dynamic myocardial T(1) mapping using a cine steady-state look-locker approach. *Magn reson med.* 2018;79(4):2087–2100. 10.1002/mrm.26887 [PubMed: 28856778]
15. Becker KM, Schulz-Menger J, Schaeffter T, Kolbitsch, C. Simultaneous high-resolution cardiac T1 mapping and cine imaging using model-based iterative image reconstruction. *Magn reson med.* 2019;81(2):1080–1091. 10.1002/mrm.27474 [PubMed: 30183094]
16. Shaw JL, Yang Q, Zhou ZW, Deng ZX, Nguyen C, Li D, Christodoulou AG. Free-breathing, non-ECG, continuous myocardial T-1 mapping with cardiovascular magnetic resonance multitasking. *Magn reson med.* 2019;81(4):2450–2463. 10.1002/mrm.27574 [PubMed: 30450749]
17. Qi H, Jaubert O, Bustin A, Cruz G, Chen H, Botnar R, Prieto C. Free-running 3D whole heart myocardial T1 mapping with isotropic spatial resolution. *Magn reson med.* 2019;82(4):1331–1342. 10.1002/mrm.27811 [PubMed: 31099442]
18. Becker KM, Blaszczyk E, Funk S, Nuesslein A, Schulz-Menger J, Schaeffter T, and Kolbitsch C. Fast myocardial T1 mapping using cardiac motion correction. *Magn reson med.* 2020;83(2):438–451. 10.1002/mrm.27935 [PubMed: 31418924]

19. Deichmann R, Haase A. Quantification of T1 Values by Snapshot-Flash Nmr Imaging. *J Magn Reson.* 1992;96(3):608–612. 10.1016/0022-2364(92)90347-A
20. Look DC, Locker DR. Time saving in measurement of NMR and EPR relaxation times. *Review of scientific instruments.* 1970;41(2):250–251. 10.1063/1.1684482
21. Slavin G On the use of the “look-locker correction” for calculating T1 values from MOLLI. *J Cardiovasc Magn Reson.* 2014;16 (Suppl 1):55. 10.1186/1532-429X-16-S1-P55 [PubMed: 25190004]
22. Stollberger R, Wach P. Imaging of the active B1 field in vivo. *Magn reson med.* 1996;35(2):246–51. 10.1002/mrm.1910350217 [PubMed: 8622590]
23. Treier R, Steingoetter A, Fried M, Schwizer W, Boesiger P. Optimized and combined T1 and B1 mapping technique for fast and accurate T1 quantification in contrast-enhanced abdominal MRI. *Magn reson med.* 2007;57(3):568–76. 10.1002/mrm.21177 [PubMed: 17326175]
24. Yarnykh VL. Actual flip-angle imaging in the pulsed steady state: a method for rapid three-dimensional mapping of the transmitted radiofrequency field. *Magn reson med.* 2007;57(1):192–200. 10.1002/mrm.21120 [PubMed: 17191242]
25. Serry FM, Ma S, Li D, Christodoulou AG. Dual flip angle IR-FLASH for B1+ insensitive T1 mapping: Application to T1 CMR multitasking. In *Proceedings of the ISMRM & SMRT Virtual Conference & Exhibition, 2020.* p 307. <https://archive.ismrm.org/2020/0895.html>
26. Pauly J, Nishimura D, Macovski A. A k-space analysis of small-tip-angle excitation. *J Magn Reson.* 1989 1 1;81(1):43–56. 10.1016/0022-2364(89)90265-5
27. Liang ZP. Spatiotemporal imaging with partially separable functions. In *Proceedings of the 4th IEEE International Symposium on Biomedical Imaging, 2007.* p 988–991. 10.1109/ISBI.2007.357020
28. Kolda TG, Bader BW. Tensor decompositions and applications. *SIAM Review.* 2009;51(3):455–500. 10.1137/07070111X
29. Chung S, Kim D, Breton E, Axel L. Rapid B1+ mapping using a preconditioning RF pulse with TurboFLASH readout. *Magn reson med.* 2010;64(2):439–46. 10.1002/mrm.22423 [PubMed: 20665788]
30. Shao J, Rapacchi S, Nguyen KL, Hu P. Myocardial T1 mapping at 3.0 tesla using an inversion recovery spoiled gradient echo readout and bloch equation simulation with slice profile correction (BLESSPC) T1 estimation algorithm. *J Magn Reson Imaging.* 2016;43(2):414–25. 10.1002/jmri.24999 [PubMed: 26214152]
31. Watson PF, Petrie A. Method agreement analysis: a review of correct methodology. *Theriogenology.* 2010;73(9):1167–79. 10.1016/j.theriogenology.2010.01.003 [PubMed: 20138353]
32. Cole TJ. Too many digits: the presentation of numerical data. *Arch Dis Child.* 2015;100(7):608–9. 10.1136/archdischild-2014-307149 [PubMed: 25877157]
33. Zhou R, Weller DS, Yang Y, Wang J, Mugler JP, Salerno M. Free-breathing continuous cine and T1 mapping acquisition using a motion-corrected dual flip angle inversion-recovery spiral technique at 3 T. In *Proceedings of the ISMRM & SMRT Virtual Conference & Exhibition, 2020.* p 314. 10.1002/mrm.27763
34. Weingartner S, Messner NM, Budjan J, Lossnitzer D, Mattler U, Papavassiliu T, et al. Myocardial T1-mapping at 3T using saturation-recovery: reference values, precision and comparison with MOLLI. *J Cardiovasc Magn Reson.* 2016;18(1):84. 10.1186/s12968-016-0302-x [PubMed: 27855705]

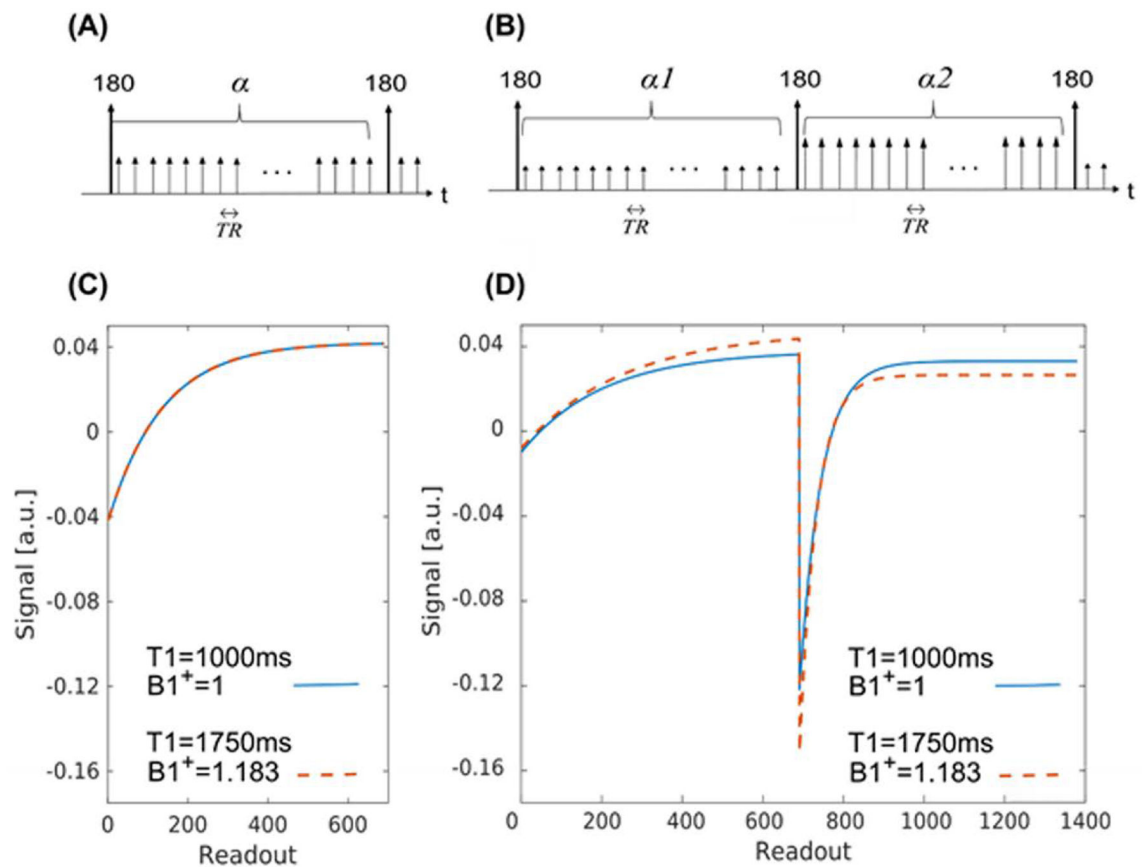


FIGURE 1.

Pulse sequence and simulated T_1 recovery curves for 1FA (A, C) and 2FA (B, D) IR-FLASH. In 2FA IR-FLASH, an inversion pulse is followed by a first train of FLASH readout pulses with the repetition time TR at the first small flip angle (FA) α_1 , then immediately by another inversion pulse and the second train of FLASH pulses at the second small FA α_2 at the same TR (B) before repeating. T_1 recovery curves for $T_1 = 1000\text{ms}$, $B_1^+ = 1.00$ and for $T_1 = 1750\text{ms}$, $B_1^+ = 1.183$ are nearly superimposed in 1FA IR-FLASH (C), but resolved in 2FA IR-FLASH (D). In this simulation, for 1FA IR-FLASH, $\alpha = 5^\circ$, and for 2FA IR-FLASH, $\alpha_1 = 3^\circ$, $\alpha_2 = 10^\circ$, the same values that were used in all experiments. Note that in the experiments, 1FA and 2FA scans were of the same duration.

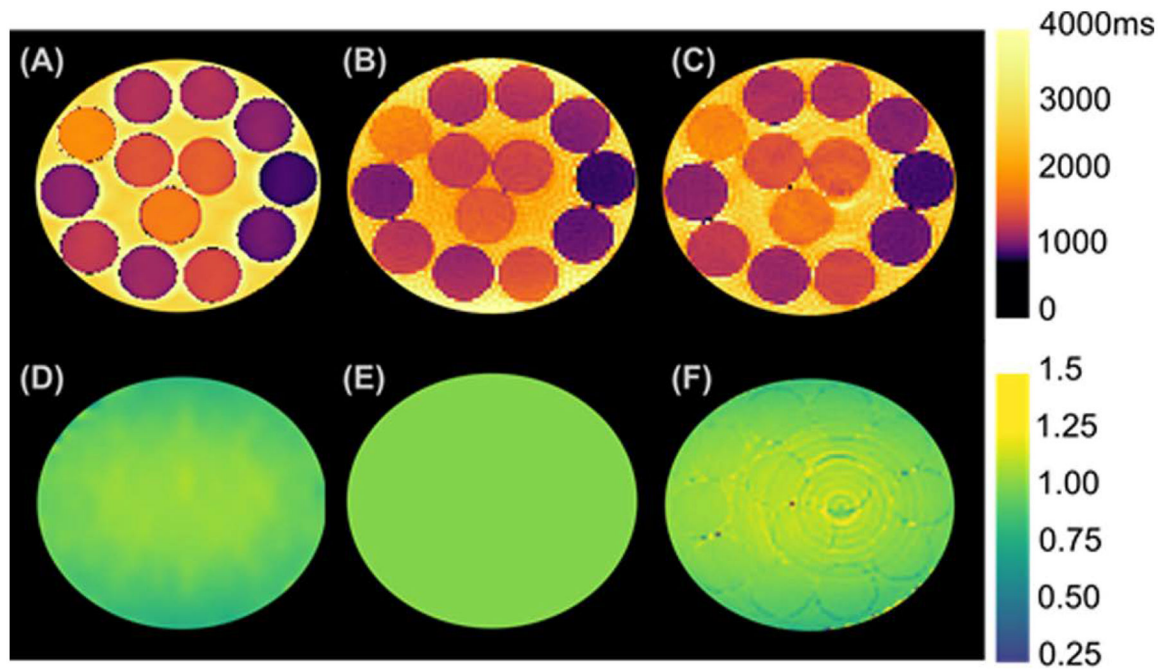


FIGURE 2.

Maps of T_1 and normalized B_1^+ from static T_1 phantom experiments. The cylindrical phantom was approximately 13.6cm diameter, fully captured in the images. IR-TSE T_1 (A), 1FA IR-FLASH T_1 (B), 2FA IR-FLASH T_1 (C), scanner-produced B_1^+ (D), simulated uniform B_1^+ ($=1$) for 1FA IR-FLASH (E), and 2FA IR-FLASH β (F) (see Theory section). In the water matrix surrounding the 13 vials, gradual decrease of T_1 values from the perimeter towards the center is present only in the 1FA T_1 map (B), absent in the 2FA T_1 map (C) and in the IR-TSE T_1 map (A). The mirror of this pattern is visible in the 2FA β map (F): gradual increase of β values from the perimeter towards the center. By fitting concurrently from the same data for T_1 and β , 2FA absorbs the artifactual T_1 variation seen in the 1FA T_1 map into the 2FA β map, thus producing a T_1 map (C) closer to the reference T_1 map of the IR-TSE scan (A), including in-vial T_1 estimates (see text, and also Figure 3).

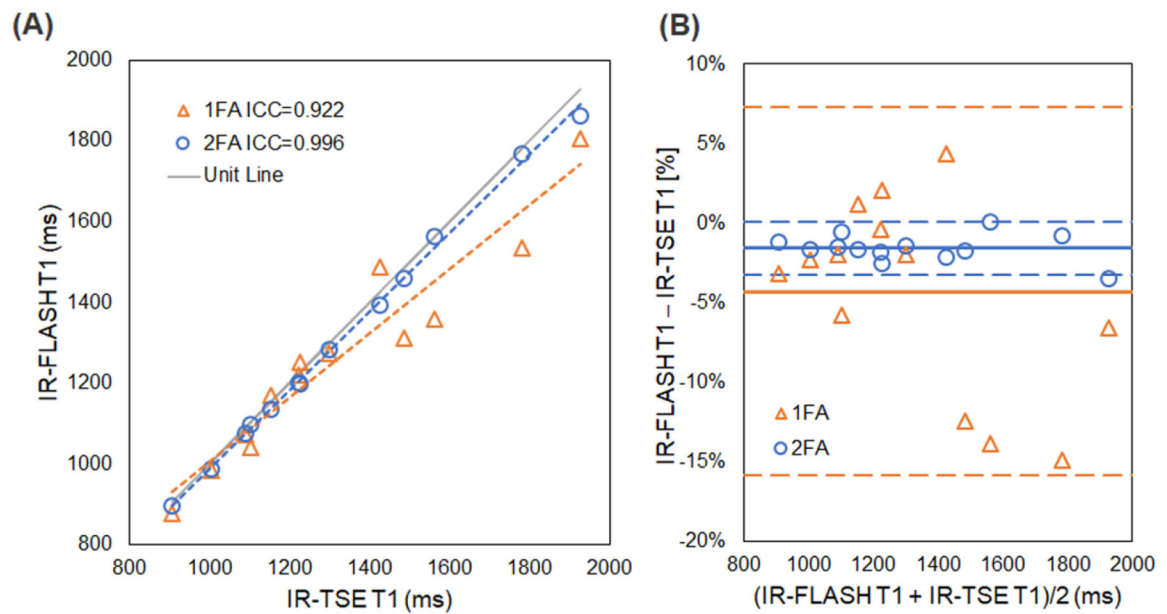
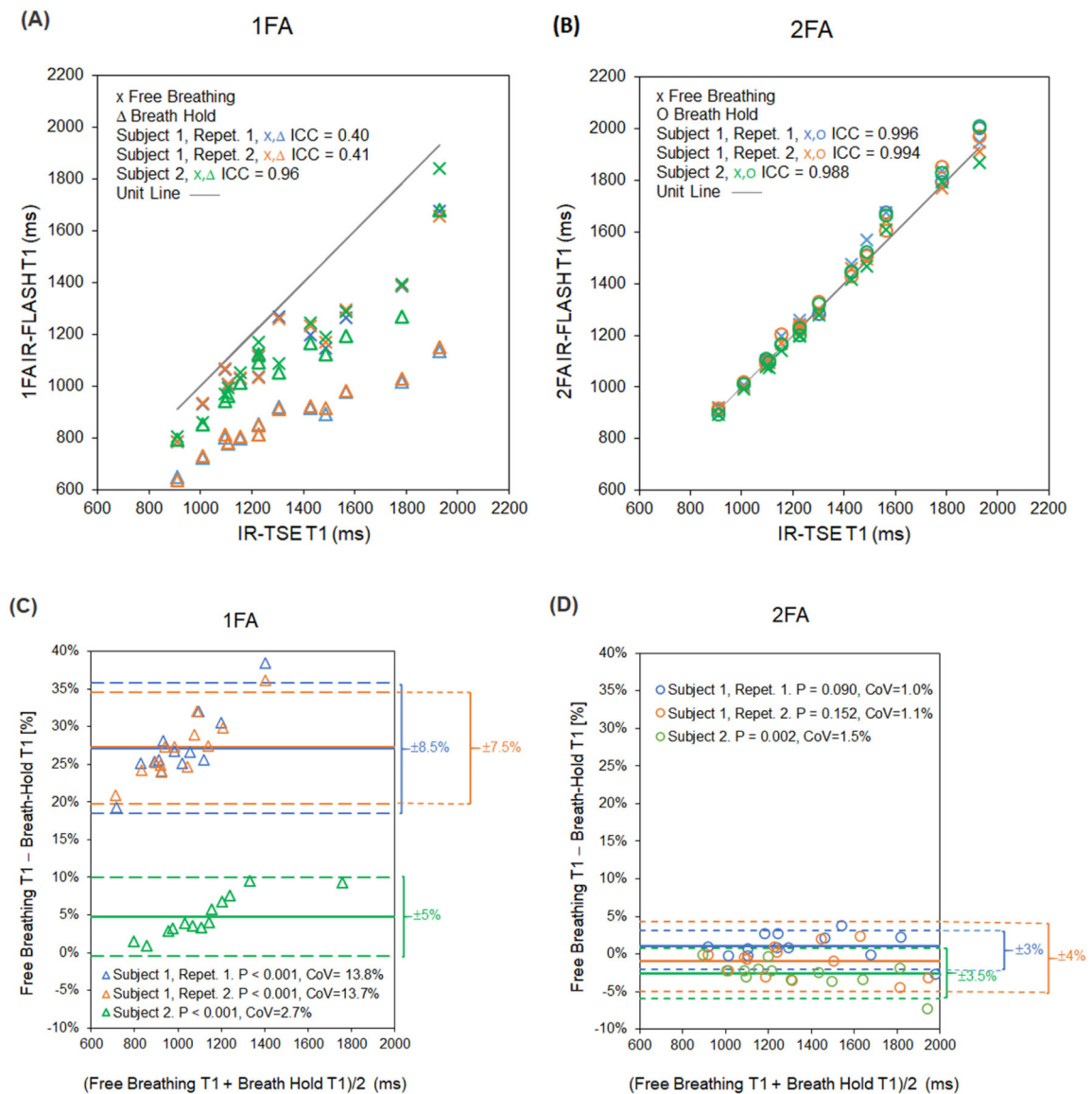


FIGURE 3.

Agreement of IR-FLASH with IR-TSE in static phantom experiments. 1FA and 2FA IR-FLASH T_1 estimates for 13 phantom vials seen in Figure 2, and linear regressions (dashed sloped lines) of the scatters; also, IR-FLASH and IR-TSE intraclass correlation coefficients (ICCs) (A). Bland-Altman plot of data in A: T_1 estimate difference (1FA IR-FLASH T_1 minus IR-TSE T_1 and 2FA IR-FLASH T_1 minus IR-TSE T_1) reported as percentage of two-method (1F IR-FLASH and IR-TSE, or 2F IR-FLASH and IR-TSE) mean T_1 values, with bias or mean difference (solid horizontal lines; -63ms , $P = 0.035$ for 1FA; -21ms , $P < 0.001$ for 2FA), and $\pm 95\%$ confidence intervals (mean $\pm 1.96 \times \text{SD}$) denoting limits of agreement (dashed horizontal lines; $\pm 57\text{ms}$ for 1FA; $\pm 10\text{ms}$ for 2FA) (B).

**FIGURE 4.**

Phantom-on-thorax breath-hold (BH) and free-breathing (FB) T_1 estimates in 2 subjects. Subject 1 was scanned twice with each protocol in the same session; subject 2 was scanned once with each protocol. The phantom had 13 vials (see Figure 2). Each of three colors represents a pair of scans: an FB scan and its counterpart BH scan; there were two such pairs for subject 1, and one pair for subject 2. Panels A and B show scatter plots of T_1 estimates from 1FA (A) and 2FA (B) IR-FLASH phantom-on-thorax scans vs. IR-TSE (phantom on scanner table scan) for 13 vials, as well as ICCs for each pair of BH-FB values. BH-FB CoVs were 11.3% for 1FA IR-FLASH and 1.2% for 2FA IR-FLASH. Panels C and D are Bland-Altman plots comparing FB to BH T_1 estimates for 1FA IR-FLASH (C) and 2FA IR-FLASH (D) scans, showing FB vs. BH biases (mean deviation; solid line) and 95% limits of agreement around the mean (dashed line); they also include BH-FB CoVs, and p -values for FB vs. BH bias.

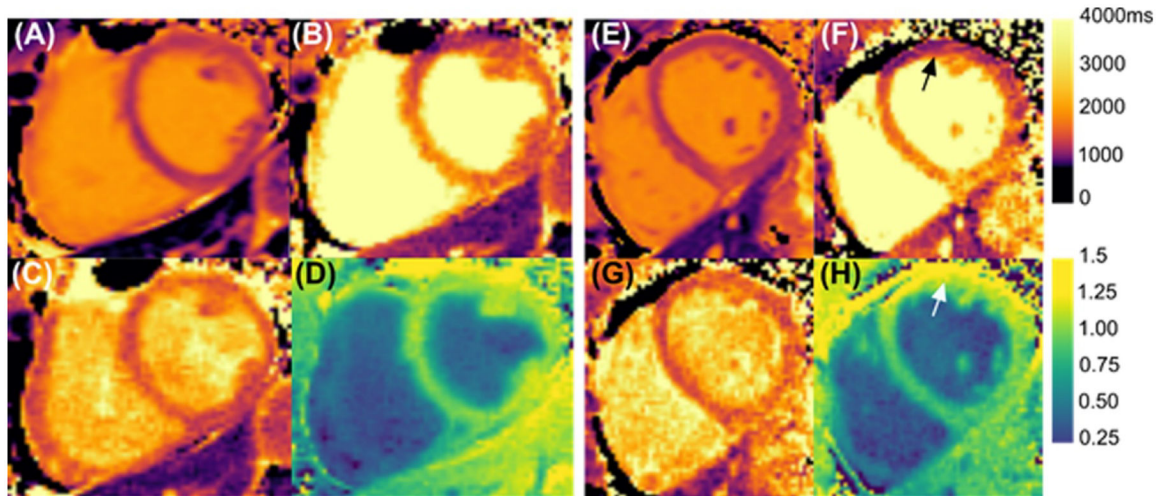


FIGURE 5.

Representative maps from 2D scans of mid-ventricular cardiac slices in end diastole in free-breathing in subject 3 (A-D) and subject 4 (E-H). MOLLI T_1 (A, E), 1FA IR-FLASH T_1 (B, F), 2FA IR-FLASH T_1 (C, G), and 2FA IR-FLASH β (normalized B_1^+) spin history (D, H). In the blood pool, T_1 estimate improved in 2FA over 1FA, and β had lower values than in the myocardium. Differences in β reflect the different spin histories (i.e., the number of excitation pulses experienced) of the blood, which flows through the slice and thus experiences fewer FLASH excitation pulses, versus of the myocardium, which, despite in-plane motion, is expected to largely remain in the slice, thus experiencing most if not nearly all the FLASH excitation pulses. For subject 4, in the anterolateral region of the myocardium, β records larger B_1^+ experienced by spins (arrow in H), possibly from abrupt susceptibility difference across the myocardium/lung boundary. 1FA underestimates T_1 in this region (arrow in F) relative to the rest of the myocardium, an artefact which is absent in 2FA T_1 (G) and MOLLI T_1 (E) maps. In this region, 2FA has absorbed this regional difference into the spin history (β) map, correcting the 1FA T_1 error.